Structure and properties of tris(tetramethylammonium) nonabromodiarsenate(III), $[(CH_3)_4N]_3[As_2Br_9]$



2007 J. Phys.: Condens. Matter 19 236221

(http://iopscience.iop.org/0953-8984/19/23/236221)

IOP PUBLISHING JOURNAL OF PHYSICS: CONDENSED MATTER

J. Phys.: Condens. Matter **19** (2007) 236221 (17pp) doi:10.1088/0953-8984/19/23/236221

# Structure and properties of tris(tetramethylammonium) nonabromodiarsenate(III), $[(CH_3)_4N]_3[As_2Br_9]$

**Maciej Wojtaś[1], Jacek Zaleski[2], Wojciech Medycki[3] and Ryszard Jakubas[1]**

[1] Faculty of Chemistry, University of Wrocław, Joliot-Curie 14, 50-383 Wrocław, Poland
[2] Institute of Chemistry, University of Opole, Oleska 48, 45-951 Opole, Poland
[3] Institute of Molecular Physics, PAS, Smoluchowskiego 17, 60-179 Poznań, Poland

E-mail: maciekwo@eto.wchuwr.pl

Received 17 November 2006, in final form 28 March 2007
Published 15 May 2007
Online at stacks.iop.org/JPhysCM/19/236221

**Abstract**

The new tetramethylammonium bromoarsenate(III) crystal $[(CH_3)_4N]_3[As_2Br_9]$ has been synthesized and its phase behaviour established by differential scanning calorimetry and dilatometry. Three phase transitions are found: at 346/346 K (I $\leftrightarrow$ II), at 165/171 K (II $\leftrightarrow$ III) and at 157/165 K (III $\leftrightarrow$ IV) on cooling/heating. Single-crystal x-ray diffraction studies of phases I (at 370 K) and II (at 298 K) have shown that the structure comprises discrete $[As_2Br_9]^{3-}$ anions and disordered $[(CH_3)_4N]^+$ cations. Phase II crystallizes in the polar space group $P31c$; its polar nature was confirmed by pyroelectric measurements. Phase I has higher symmetry, $P6_3mc$ or $P\bar{6}2c$. Dielectric dispersion measurements revealed a relaxation process in the crystal. The ferroic (ferroelastic) properties were found below 165 K (the II $\rightarrow$ III transition). The NMR studies indicate the subtle change in the motional state of the tetramethylammonium cations through all observed phase transitions.

## 1. Introduction

Halogenoantimonates(III) and halogenobismuthates(III) of a general formula $R_aM_bX_{3b+a}$ (where R denotes organic cations, M = Sb, Bi and X = Cl, Br, I) are the subjects of recent experimental interest because they exhibit frequently both ferroelectric and ferroelastic properties [1–6]. These salts are characterized by a rich diversity of the anionic form. The ferroelectricity is limited, however, to the compounds crystallizing with the $R_3M_2X_9$ [7] and $R_5M_2X_{11}$ [8, 9] compositions. For the $R_3M_2X_9$ subgroup of salts there were found four various types of connections of octahedral $MX_6$ units to each other: (i) one-dimensional structure (double zigzag anionic chains) [10], (ii) polyanionic two-dimensional layers [11],

  

(iii) discrete bioctahedral [12] and (iv) isolated tetrameric units [13]. The most interesting are the $R_3M_2X_9$ salts of type (ii), for which ferroelectricity has some tendency to appear. Numerous experimental studies on this type of salts showed that the size and symmetry of the cations and their ability to form hydrogen bonds influence the structure of the anionic sublattice. Small organic cations like monomethyl-, dimethyl- and trimethylammonium embedded in the crystal structure quite frequently lead to the two-dimensional layers of polyhedral network (ii), and, solely in this case, if salts crystallize in the $R_3M_2X_9$ stoichiometry, the ferroelectricity may appear. The embedding in the crystal structure of bulky organic cations such as the tetramethylammonium one leads to the breaking of the polymeric anionic structure and disappearance of ferroelectricity [14, 15]. On the other hand, very little is known about the structural and physical properties of halogenoarsenates(III). Until now only two molecular–ionic chloroarsenate(III) derivatives have been studied systematically from the point of view of dynamic properties and possible structural phase transitions: $[(CH_3)_2NH_2]_3As_2Cl_9$ [16] and $[(CH_3)_4N]_3As_2Cl_9$ [17]. It is interesting that tetramethylammonium analogues, similarly to the corresponding halogenoantimonates(III) and halogenobismuthates(III), are characterized by a discrete bioctahedral $[M_2Br_9]^{3-}$ units in the crystal lattice. $[(CH_3)_4N]_3As_2Cl_9$ was found to be a ferroic crystal, since it displays ferroelastic properties below 146 K. However, it should be added that at room temperature it crystallizes in the polar space group $P31c$. The tetramethylammonium analogues with various anionic moieties were found to be promising because of their interesting ferroelectric properties and incommensurable modulated structures, for example the best known $[(CH_3)_4N]_2[BX_4]$ type crystals (where B = bivalent metal and X = halogen) [18–21]. Most of the tetramethylammonium salts from halogenoantimonates(III) and halogenobismuthates(III) possess the pyroelectric and ferroelastic properties in their ordered low temperature phases [22]. In the search for polar materials within the halogenoarsenate(III) salts a new tetramethylammonium derivative, $[(CH_3)_4N]_3[As_2Br_9]$, was synthesized.

In this paper we report the structural characterization of $[(CH_3)_4N]_3[As_2Br_9]$ at two temperatures in various phases. These phases are briefly compared and mechanism of the phase transition taking place in this crystal is proposed on the basis of the calorimetric, dilatometric and dielectric measurements.

## 2. Experimental details

Tris(tetramethylammonium) nonabromodiarsenate(III) was prepared by mixing in stoichiometric proportions of tetramethylammonium hydrobromide (99% Aldrich) and arsenic(III) oxide (99.99% Aldrich) in concentrated hydrobromic acid. The obtained compound was recrystallized and single crystals of $[(CH_3)_4N]_3[As_2Br_9]$ were grown by slow evaporation at 300 K from aqueous solution. The chemical formula of the compound was checked by elemental analysis (found: C, 13.32; H, 3.41; N, 3.87%; calculated: C, 13.21; H, 3.33; N, 3.85%).

Single-crystal x-ray diffraction at the temperatures 298 and 370 K was performed on an Xcalibur CCD diffractometer with graphite monochromated Mo K$\alpha$($\lambda$ = 0.710 73 Å) radiation. The reflections were measured using the $\omega$-scan technique with $\Delta\omega = 0.75°$ and $\Delta t = 20$ s. The structures were solved by the Patterson method. All of the data were subjected to Lorentz, polarization and semi-empirical absorption corrections based on symmetry-equivalent reflections [23]. All hydrogen atoms were added using the standard geometric criteria, then refined using the riding model and constrained to a distance of 0.96 Å for $CH_3$ groups. Their displacement parameters were taken with coefficients 1.5 times larger than the respective parameters of the nitrogen and carbon atoms. The Oxford Diffraction software CrysAlis CCD and CrysAlis RED programs were used during the data

collection, cell refinement and data reduction processes [23]. The SHELXS-97 and SHELXL-97 programs [24, 25] were used for the structure solution and refinement. The structure drawings were prepared using the SHELXTL program [26].

Crystallographic data (excluding structure factors) for the structure at 298 and 370 K have been deposited at the Cambridge Crystallographic Data Centre as supplementary publications CCDC 620101 and 620102, respectively. Copies of the data can be obtained, free of charge, on application to the Director, CCDC, 12 Union Road, Cambridge CB2 1EZ, UK (fax, int. code+(1223) 336033, or e-mail, data_request@ccdc.cam.ac.uk).

The complex dielectric permittivity, $\epsilon^* = \epsilon' - i\epsilon''$, was measured with an HP 4285A precision $LCR$ meter in the frequency range between 75 kHz and 15 MHz and in the 100–400 K range. The dimensions of the sample were of the order of $5 \times 5 \times 1$ mm$^3$. The overall error for the real and imaginary parts of the complex electric permittivity was less than 5 and 10%, respectively.

The spontaneous polarization was measured between 100 and 240 K by a charge integration technique using a Keithley 617 programmable electrometer. The temperature was stabilized by an Instec STC 200 temperature controller.

Differential scanning calorimetry (DSC) measurements were carried out using a Perkin Elmer DSC-7 in the temperature range 100–450 K.

The dilatometric measurements were carried out by a Perkin Elmer TMA-7 thermomechanical analyser between 100 and 450 K. The dimensions of the sample were of the order of $8 \times 5 \times 1.5$ mm$^3$.

The ferroelastic domain structure of the crystal was studied by means of a PZO Warszawa optical polarization microscope. The samples were placed in a LINKAM THM-600 heating/cooling stage, where the temperature was stabilized to within 0.1 K.

The spin–lattice relaxation time measurements were performed at 90 MHz using an SXP 4–100 Bruker pulse spectrometer employing a $\pi$–$\theta$–$\pi/2$ pulse sequence. Before use the sample was dried under $10^{-3}$ Torr vacuum for several hours at room temperature. The measurements were made between 77 and 360 K. The temperature control system used was a Bruker B–ST 100/700 controller. Most of the measurements were repeated two or three times and found to be well reproducible. For all data reported, the magnetization was found to recover exponentially. The second moment of NMR lines for protons was found on the basis of analysis of the solid echo shape.

## 3. Results and discussion

### *3.1. DSC and dilatometric measurements*

Figure 1 presents the results of differential scanning calorimetry measurements. Over the high temperature region a reversible phase transition is observed, which is manifested as a clear deflection of the baseline at $T_{c1} = 346$ K, both on cooling and heating. The lack of the temperature hysteresis and the shape of this thermal anomaly point out the continuous character of this phase transition. In the low temperature region we deal with two phase transitions manifested as two thermal anomalies. The overlapping peaks were fitted with two Gauss-type curves, which enabled us to estimate the $\Delta H$ of both phase transitions. The temperatures of these phase transitions are $T_{c2} = 165/171$ K and $T_{c3} = 157/165$ K (cooling/heating). The transition entropy, $\Delta S_2$, equals 5.5 J mol$^{-1}$ K$^{-1}$, whereas $\Delta S_3$ is 2.8 J mol$^{-1}$ K$^{-1}$. The value of $\Delta S_2$ equals, in the error limit, $R\ln 2$ and the sum $\Delta S_2 + \Delta S_3 \approx R\ln 3$. In the case of these two transitions the presence of temperature hysteresis as well as the shape of the thermal anomalies (peaks) show that both low temperature phase transitions are discontinuous. In turn the values

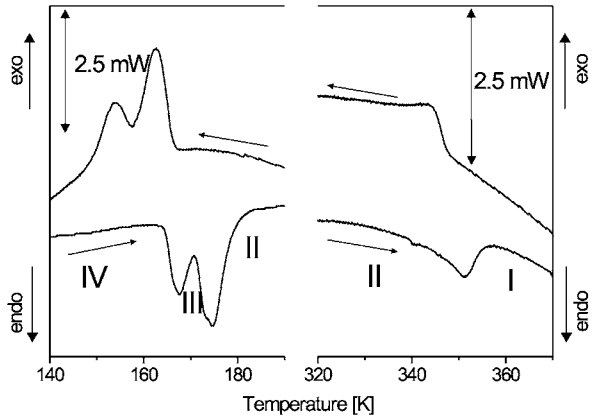


**Figure 1.** DSC curves of $[(CH_3)_4N]_3[As_2Br_9]$ crystal.

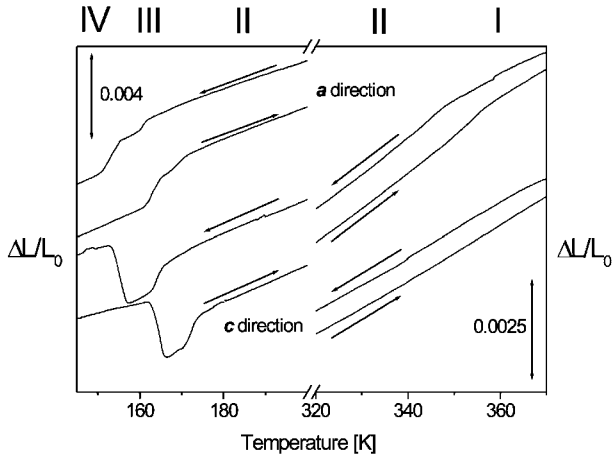


**Figure 2.** Dilatometric curves of $[(CH_3)_4N]_3[As_2Br_9]$ crystal along $a$ and $c$ directions.

of $\Delta S_2$ and $\Delta S_3$ incontrovertibly show evidence of an order–disorder character of these low temperature phase transitions.

In figure 2 results of linear thermal expansion are presented. The measurements were carried out along the $a$ and $c$ directions. The high temperature phase transition is manifested only as a very subtle anomaly of the $\Delta L/L_0$ representing the $c$-direction, and the mean thermal expansion coefficient, $\overline{\alpha}_c = \Delta L/L\Delta T$, remains constant above and below the phase transition temperature. The phase transition is manifested more strongly along the $a$-axis: quite a clear change in the $\overline{\alpha}_a$ coefficient above and below the phase transition point, i.e. 346 K, can be observed. In contrast to calorimetric measurements, some temperature hysteresis is observed, but this is the result of the heterogenous distribution of temperature within the sample.

The low temperature phase transitions are unambiguously manifested due to the change of $\Delta L/L_0$ at the phase transition temperature along the $a$ and the $c$ directions. It is interesting that the phase transition at $T_{c2}$ is accompanied by a smaller change in the length of crystal than at $T_{c3}$ along both axes. Simultaneously, in the $a$ direction both transitions cause a decrease in the length of the crystal on cooling, whereas in the $c$ direction the phase transition II $\rightarrow$ III is accompanied by a decrease of $\Delta L/L_0$ value that increases at $T_{c3}$. It is worth noting that the

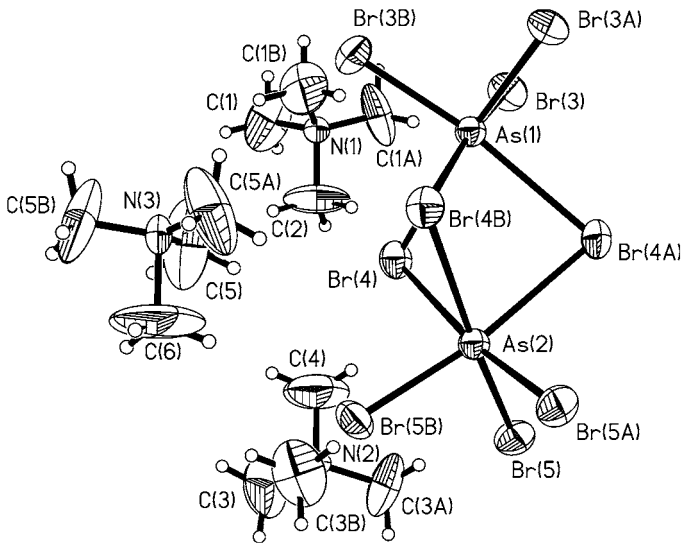


**Figure 3.** Atom numbering scheme of the $[(CH_3)_4N]_3[As_2Br_9]$ crystal at 298 K.

temperature coefficients, $\alpha$, for both $a$ and $c$ axes are positive in the low, as well as in the high, temperature region.

The results of the dilatometric measurements are in good agreement with those obtained by means of the DSC. The following sequence of the phase transition is observed:

$$\mathrm{IV} \underset{165}{\overset{157}{\rightleftharpoons}} \mathrm{III} \underset{171}{\overset{165}{\rightleftharpoons}} \mathrm{II} \underset{346}{\overset{346}{\rightleftharpoons}} \mathrm{I}$$

discontinuous discontinuous continuous

### *3.2. Crystal structure of* $[(CH_3)_4N]_3[As_2Br_9]$

We undertook x-ray crystal structure determinations of $[(CH_3)_4N]_3[As_2Br_9]$ at 370 K (phase I), 298 K (phase II) and low temperature (phase IV). The latter study was unsuccessful due to twinning of the crystal (see section 3.5). The structure of phase II was successfully solved in the polar, trigonal space group $P31c$. Phase I, which exists above $T_{c1}$, evidently has higher symmetry, which could not be unambiguously determined because of large dynamic disorder of cations. From observations under the polarizing microscope it must be trigonal or hexagonal. The structure could be successfully solved in space groups $P6_3mc$ (no 186) and $P\bar{6}2c$ (no 190), refinement in which gave practically equal values of $R$ (2.48 and 2.50%, respectively). In $P6_3mc$ the asymmetric unit comprises two As and three Br atoms and three cations, of which two are disordered. In $P\bar{6}2c$ there are one As and two Br atoms and two cations, one of which is disordered. An increase of symmetry from phase II to phase I seems to agree with their optical properties (see section 3.5). Crystal data of phases II and I (in $P6_3mc$) are listed in table 1, bond distances and angles in table 2; the atom numbering and crystal packing of phase II are shown in figures 3 and 4.

The crystal structure in phase II is built up from discrete bioctahedral units $[As_2Br_9]^{3-}$ and tetramethylammonium cations $[(CH_3)_4N]^+$. Such a structure is common among pnicogen and halogen salts with tetramethylammonium cations [1, 17]. The anionic and cationic sublattices are bonded via electrostatic interactions.

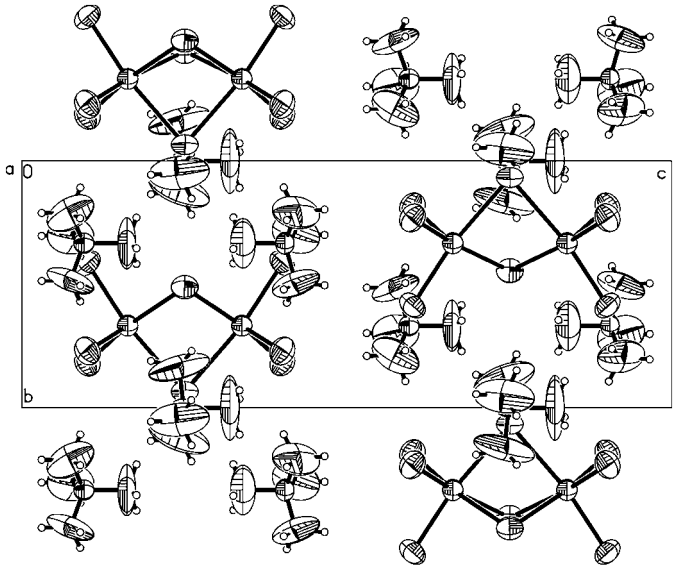


**Figure 4.** The view of the $[(CH_3)_4N]_3[As_2Br_9]$ crystal structure at 298 K along the $a$-axis. Thermal ellipsoids are in 50% probability.

**Table 1.** Crystal data and structure refinement for $[(CH_3)_4N]_3[As_2Br_9]$ at 298 K (phase II) and tentative data at 370 K (phase I).

| | | |
|---|---|---|
| Empirical formula | C12 H36 As2 Br9 N3 | |
| Formula weight | 1091.47 | |
| Temperature | 298(2) K | 370.0(1) K |
| Wavelength | 0.710 73 Å | |
| Crystal system, space group | Trigonal, $P31c$ | Hexagonal, $P6_3mc$ |
| Unit cell dimensions | $a = 9.4873(6)$ Å | $a = 9.5515(8)$ Å |
| | $c = 21.6743(18)$ Å | $c = 21.790(2)$ Å |
| Volume | 1689.5(2) Å$^3$ | 1721.6(3) Å$^3$ |
| $Z$, calculated density | 2, 2.145 Mg m$^{-3}$ | 2, 2.106 Mg m$^{-3}$ |
| Absorption coefficient | 12.626 mm$^{-1}$ | 12.390 mm$^{-1}$ |
| $F(000)$ | 1020 | |
| Crystal size | 0.10 mm × 0.13 mm × 0.13 mm | |
| Θ range for data collection | 2.7°–27.5° | 3.1°–27.5° |
| Index ranges | $-11 \leqslant h \leqslant 12$, $-12 \leqslant k \leqslant 11$, $-27 \leqslant l \leqslant 28$ | $-10 \leqslant h \leqslant 12$, $-12 \leqslant k \leqslant 10$, $-28 \leqslant l \leqslant 28$ |
| Reflections collected/unique | 12 218/2524 ($R_{(int)} = 0.033$) | 12 519/1562 ($R_{(int)} = 0.064$) |
| Absorption correction | Semi-empirical from equivalents | |
| Max. and min. transmission | 0.365 and 0.291 | 0.290 and 0.274 |
| Refinement method | Full-matrix least squares on $F^2$ | |
| Data/restraints/parameters | 2524/1/79 | 1562/1/64 |
| Goodness of fit on $F^2$ | 0.91 | 0.71 |
| Final $R$ indices [$I > 2\sigma$(I)] | $R_1 = 0.0314$, $wR_2 = 0.0633$ | $R_1 = 0.0242$, $wR_2 = 0.0567$ |
| $R$ indices (all data) | $R_1 = 0.0634$, $wR_2 = 0.0620$ | $R_1 = 0.1218$, $wR_2 = 0.0503$ |
| Absolute structure parameter | 0.06(4) | 0.00 |
| Largest diff. peak and hole | 0.49 and $-0.47e$ Å$^{-3}$ | 0.31 and $-0.20e$ Å$^{-3}$ |

The anion $[As_2Br_9]^{3-}$ consists of two $AsBr_6$ face-sharing octahedra characterized by three terminal and three bridging As–Br bonds. The octahedra are deformed because each terminal

**Table 2.** Selected bond lengths and angles for $[(CH_3)_4N]_3[As_2Br_9]$ at 298 and 370 K.

| 298 K | | | |
|---|---|---|---|
| As(1)–Br(3) | 2.4750(11) | Br(3)–As(1)–Br(4) | 91.85(2) |
| As(1)–Br(4) | 2.9026(11) | Br(4)$^1$–As(1)–Br(4) | 82.05(3) |
| As(2)–Br(5) | 2.4790(11) | Br(5)$^1$–As(2)–Br(5) | 93.09(5) |
| As(2)–Br(4) | 2.9028(12) | Br(5)–As(2)–Br(4) | 91.94(2) |
| Br(3)$^1$–As(1)–Br(3) | 93.15(5) | Br(5)–As(2)–Br(4)$^1$ | 172.34(4) |
| Br(3)–As(1)–Br(4)$^1$ | 172.27(4) | Br(4)–As(2)–Br(4)$^1$ | 82.06(3) |
| Br(3)$^1$–As(1)–Br(4) | 92.45(2) | As(1)–Br(4)–As(2) | 81.43(2) |
| Symmetry transformations used to generate equivalent atoms | | | |
| $^1 -x+y+1, -x+1, z$ | | $^2 -y+1, x-y, z$ | $^3 -y+2, x-y, z$ |
| $^4 -x+y+2, -x+2, z$ | | $^5 -y+1, x-y-1, z$ | |
| 370 K | | | |
| As(1)–Br(3) | 2.479(4) | Br(3)–As(1)–Br(4) | 92.15(10) |
| As(1)–Br(4) | 2.941(5) | Br(4)$^2$–As(1)–Br(4) | 81.18(15) |
| Br(4)–As(2) | 2.898(4) | As(2)–Br(4)–As(1) | 81.63(3) |
| As(2)–Br(5) | 2.475(4) | Br(5)–As(2)–Br(5)$^1$ | 92.6(2) |
| Br(3)–As(1)–Br(4)$^2$ | 171.2(2) | Br(5)–As(2)–Br(4)$^1$ | 173.1(2) |
| Br(3)$^1$–As(1)–Br(3) | 93.9(2) | Br(5)–As(2)–Br(4) | 92.18(11) |
| Br(4)$^1$–As(2)–Br(4) | 82.63(15) | | |
| Symmetry transformations used to generate equivalent atoms | | | |
| $^1 -y+1, x-y+1, z$ | | $^2 -x+y, -x+1, z$ | $^3 -y+1, x-y, z$ |
| $^4 -x+y+1, -x+1, z$ | | $^5 -y+2, x-y+1, z$ | |

bond is opposite to the bridging one and the bridging bonds are longer than the terminal ones. This is also the case for other halogenoarsenates(III) or halogenoantimonates(III) [1]. This difference equals about 0.4 Å (see table 2) in the studied structure. Both octahedra are slightly distorted; the angles vary from 82.06(3)° to 93.15(5)° for Br–As(1)–$Br_{cis}$ and from 82.06(3)° to 93.09(5)° for Br–As(2)–$Br_{cis}$.

The comparison of displacement ellipsoids of anion atoms, As and Br, and cation atoms, N, C and H, leads to the conclusion that the anionic sublattice is ordered; cations however may reorientate. The thermal ellipsoids of carbon atoms are distinctly bigger than the ellipsoids of other atoms and this is particularly well visible for the C(5) and C(6) carbon atoms. Such a situation—rigid anionic sublattice and dynamically disordered cations—has already been observed in $[(CH_3)_2NH_2]_3[As_2Cl_9]$ [16] and $[(CH_3)_4N]_3[As_2Cl_9]$ [17] and is also common for halogenoantimonates(III) and halogenobismuthates(III) [1, 27].

The dielectric relaxation observed in the $[(CH_3)_4N]_3[As_2Br_9]$ crystal implies that the tetramethylammonium cations should be distorted—deformed from the ideal tetrahedron. However, due to significant disorder of the tetramethylammonium cations the N–C distances could be determined only roughly. The average magnitude of these distances is about 1.45 Å at room temperature, which is the typical C–N bond length in the tetramethylammonium cation and has often been reported [28–31].

### *3.3. Pyroelectric measurements*

The x-ray studies showed that the $[(CH_3)_4N]_3[As_2Br_9]$ crystal is polar over phase II and probably non-centrosymmetric over phase I. The measurements of pyroelectric current were carried out in the vicinity of the I ↔ II and the II ↔ III ↔ IV phase transitions.

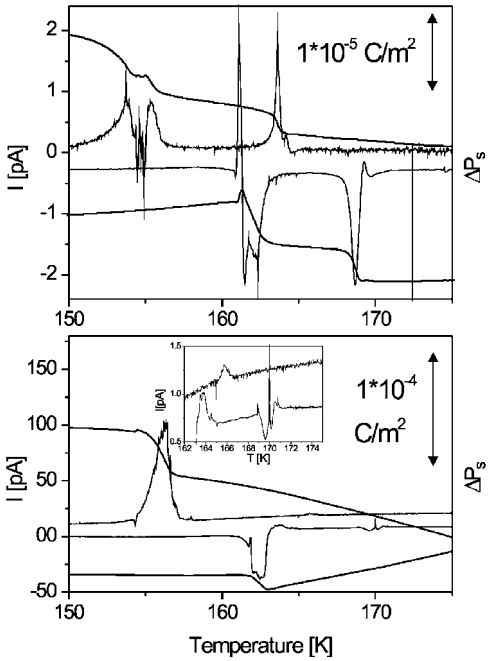


**Figure 5.** The temperature dependence of the pyroelectric current, $I$, and the spontaneous polarization change, $\Delta P_s$, measured along the $a$-axis (at the top) and the $c$-axis (at the bottom) of $[(CH_3)_4N]_3[As_2Br_9]$ in the vicinity of the low temperature phase transitions. The inset presents the temperature range around II $\leftrightarrow$ III in magnification.

Nonetheless, the I $\leftrightarrow$ II phase transition occurs from one polar phase to another and the phase transition might be manifested in the pyroelectric current versus temperature curve. This is because the experimental set-up of the pyroelectric current measurement allows us to measure the relative spontaneous polarization value. Unfortunately, the electric conductivity of the crystal above room temperature is so large that it masks other effects, including the pyroelectric current.

Figure 5 shows results of the pyroelectric current measurements in the vicinity of the II $\leftrightarrow$ III $\leftrightarrow$ IV phase transitions. The studies were performed in the $a$ and $c$ directions. Both phase transitions, II $\leftrightarrow$ III and III $\leftrightarrow$ IV, are manifested as current flow in the $a$ and the $c$ directions. It should be noted that the II $\leftrightarrow$ III phase transition pyroelectric current along the $c$-axis is also observed (see the inset of figure 5(b)), but is about two orders of magnitude smaller than this effect for the III $\leftrightarrow$ IV phase transition. The relative change in the spontaneous polarization in the $a$ direction, $\Delta P_s^a$, is equal to $1 \times 10^{-5}$ C m$^{-2}$, which is a value typical for pyroelectric materials. It should be emphasized, however, that along the $c$-axis the value of the $\Delta P_s^c$ of the III $\leftrightarrow$ IV phase transition measured on the virgin sample reaches $1 \times 10^{-4}$ C m$^{-2}$, which is a value encountered for 'weak' ferroelectrics.

The values of current and $\Delta P_s$ recorded in the $a$ direction are easily reproducible, whereas in the $c$ direction the values on heating are smaller. The reasonable explanation of this situation is cracking of the sample undergoing (after crossing) the II $\leftrightarrow$ III $\leftrightarrow$ IV phase transitions. This effect weakens the contact between the electrodes (silver paste) and the crystal surface and therefore the effective area of the crystal is smaller than it was on cooling. Values of pyroelectric current and spontaneous polarization on the next scans become equal on cooling and heating, but do not reach as high a magnitude as the virgin sample. Unfortunately, $\Delta P_s^c$ was of the order

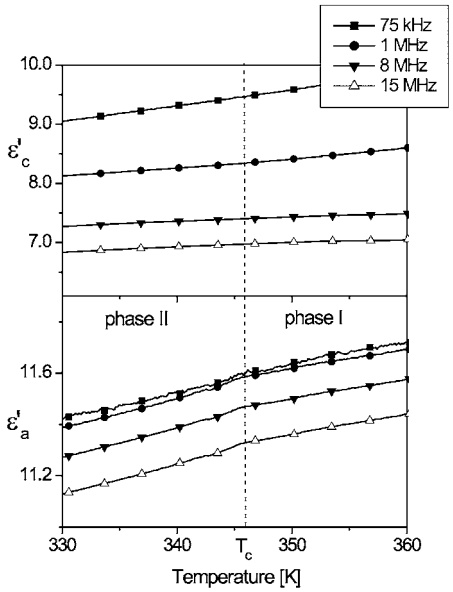


**Figure 6.** The electric permittivity versus temperature of $[(CH_3)_4N]_3[As_2Br_9]$ measured along the *c* and *a* axes in the upper and the lower graphs, respectively.

of $1 \times 10^{-4}$ C m$^{-2}$ only in the case of the virgin crystal. Because of this we were not able to study the reversibility of the spontaneous polarization under the external electric dc field—the following scans resulted in smaller $\Delta P_s$ values.

### *3.4. Dielectric studies*

The purpose of the dielectric dispersion measurements was to determine the dynamics of the dipole groups in the vicinity of the structural phase transitions. The measurements of the complex electric permittivity, $\epsilon^* = \epsilon' + i\epsilon''$, of $[(CH_3)_4N]_3[As_2Br_9]$ as a function of temperature and frequency (75 kHz–15 MHz) were performed along the *a* and *c* axes.

The real parts of the electric permittivity, $\epsilon'$, versus temperature measured in *a* and *c* directions are presented in figure 6. The phase transition at 346 K is manifested only in the *a* direction—a slight deflection of the $\epsilon'_a$ versus $T$ curve is observed. In the *c* direction practically no effect assigned to the phase transition can be noticed. It is worth noting that the values of electric permittivity along the *a* axis are higher then those recorded along the *c* axis.

A much more interesting electrical response for the $[(CH_3)_4N]_3[As_2Br_9]$ crystal is disclosed in the low temperature region. Figure 7 presents the real and imaginary parts of electric permittivity recorded along the *a* and *c* axes. One can observe the relaxation process over phase II. It is clearly seen that we deal with two dielectric relaxators. The dielectric response in the $[(CH_3)_4N]_3[As_2Br_9]$ salt is well described by the Cole–Cole relation for two independent relaxators [32]:

$$\epsilon^* = \epsilon_\infty + \frac{\Delta\epsilon_1}{1 + (i\omega\tau_1)^{1-\alpha_1}} + \frac{\Delta\epsilon_2}{1 + (i\omega\tau_2)^{1-\alpha_2}}, \tag{1}$$

where $\Delta\epsilon_i$ is the difference of $\epsilon_{0_i}$ and $\epsilon_{\infty_i}$, which in turn are the low and high frequency limits of the electric permittivity, respectively, $\omega$ is the angular frequency, $\tau_i$ are the macroscopic relaxation times and $\alpha_i$ denote the parameters of the distribution of the relaxation times.

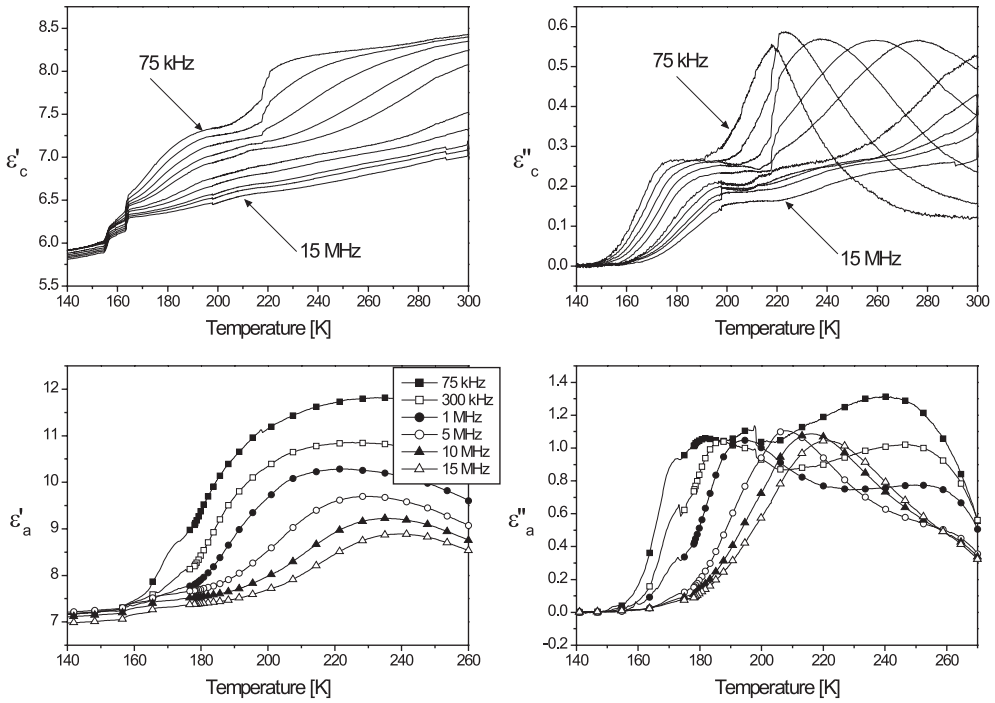


**Figure 7.** The real and imaginary parts of the complex electric permittivity versus temperature of $[(CH_3)_4N]_3[As_2Br_9]$ measured along the *c* and *a* axes in the upper and the lower graphs, respectively.

The Cole–Cole plots at selected temperatures are presented in figure 8. We have fitted the experimental Argand plots at several temperatures with equation (1) and determined the fitting parameters $\epsilon_0$, $\epsilon_\infty$ and $\tau$ for two relaxators. The activation energy, $E_a$, was estimated from the Arrhenius relation for the relaxation time:

$$\tau_i = C \exp\left(\frac{E_{a_i}}{kT}\right), \tag{2}$$

where $C$ is a constant. This activation energy estimated for the relaxation process is equal to 20 kJ mol$^{-1}$ and 12 kJ mol$^{-1}$ for relaxators 1 and 2, respectively, and is typical for the ionic crystals containing bulky organic cations.

The electric response of the $[(CH_3)_4N]_3[As_2Br_9]$ crystal along the *a*-axis is quite similar, and we also observe two relaxation processes over phase II (see figure 7 at the bottom). It is worth noting that the value of electric permittivity recorded along the *a* direction amounts to 12 units and is higher than those values observed along the *c* direction, which do not exceed 8.5 units.

At the II $\leftrightarrow$ III and III $\leftrightarrow$ IV phase transition temperatures we observe stepwise changes in both $\epsilon'_a$ and $\epsilon'_c$ values. The dielectric increment, $\Delta\epsilon$, is equal to about 0.25 units along the *c*-axis and a little bit less along the *a*-axis. Such a dielectric response, $\Delta\epsilon(T)$, is typical for a first-order phase transition, which seems to be consistent with the DSC and dilatometric results.

### *3.5. Optical observations*

Microscopic observations of the $[(CH_3)_4N]_3[As_2Br_9]$ single crystal in the plane (001) (the direction corresponds to that taken for the trigonal room temperature phase) showed a clear

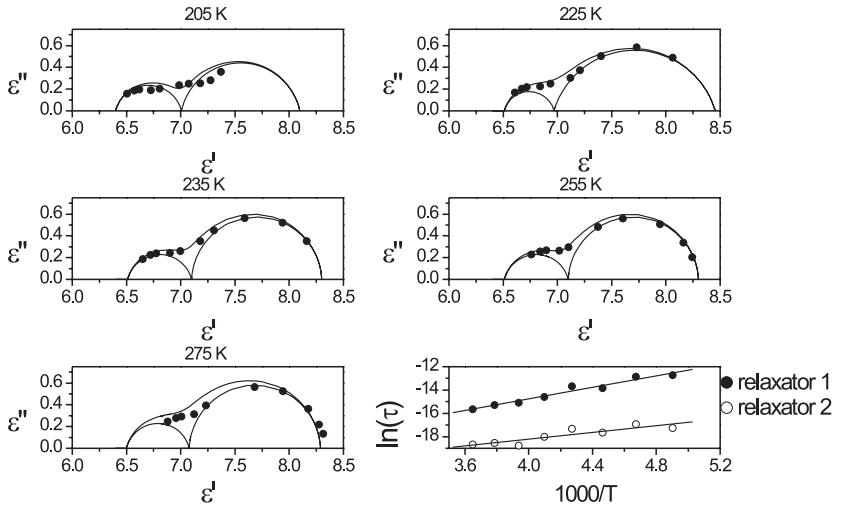


**Figure 8.** The Cole–Cole plots of the $[(CH_3)_4N]_3[As_2Br_9]$ crystal for ($\epsilon'$ and $\epsilon''$) measured in the $c$ direction at selected temperatures, and $\ln(\tau)$ versus reciprocal temperature.

ferroelastic domain structure. Figure 9 presents the micrograph of $[(CH_3)_4N]_3[As_2Br_9]$ taken in phase IV and in the vicinity of the II $\leftrightarrow$ III $\leftrightarrow$ IV phase transitions. It should be mentioned that optical observations unambiguously confirmed the existence of II $\leftrightarrow$ III and the ferroelastic domain structure was observed already in phase III. The phase front was observed exactly at 165 K on cooling and at 167 K on heating. The scan rate was 0.5 K min$^{-1}$ and these findings were easily reproducible. The III $\leftrightarrow$ IV phase transition was not visible by means of polarization microscope even at very slow temperature change (0.5 K min$^{-1}$); neither the phase front nor changes in the ferroelastic domain structure were observed. Nonetheless the process of appearance of the domain structure in phase III and its disappearance in phase II was perfectly reversible. This means that the transition may be classified as a ferroelastic one and should be accompanied by a change in the crystal symmetry [33]. It is also consistent with the single-crystal x-ray studies at low temperature.

The picture of the $[(CH_3)_4N]_3[As_2Br_9]$ crystal in phase IV (see figure 9(a)) presents the ferroelastic domain structure. The ferroelastic domains are oriented parallel to the edges of the crystal and their boundaries cross at an angle of 60 or 120°. Figures 9(b) and (c) show the process of heating the crystal sample and the phase front motion—the ferroelastic domain structure on the edges of the crystal takes the longest time to disappear. It is worth noting that two oblique cracks are present across the sample. These cracks appeared when the virgin crystal was cooled down through the II $\leftrightarrow$ III $\leftrightarrow$ IV phase transitions for the first time.

The I $\rightarrow$ II phase transition in $[(CH_3)_4N]_3[As_2Br_9]$ is undoubtedly a nonferroelastic transition. This means that such a transition must take place between hexagonal or trigonal symmetry (I) and trigonal symmetry (II). Moreover, as the I $\rightarrow$ II phase transition is continuous, a group–subgroup relation may be expected, G(I) $\supset$ G(II), and there should not be an intermediate group G$'$ such that G(I) $\supset$ G$'$ $\supset$ G(II). These conditions are totally fulfilled, among other things, by the $P6_3mc$ or $P\overline{6}2c$ space group, i.e. space groups suggested for phase I (see section 3.2). An increase in the number of atoms per unit cell is not probable in the phase transitions II $\rightarrow$ III $\rightarrow$ IV, because the micrographs show patterns indicating a proper rather than a pseudoproper ferroelastic behaviour.

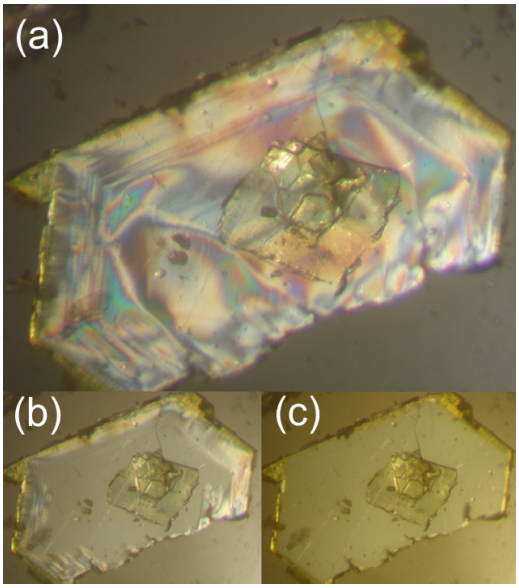


**Figure 9.** A micrograph of ferroelastic domains of $[(CH_3)_4N]_3[As_2Br_9]$ between crossed polarizers taken in the (001) plane. (a) The crystal sample in the ferroelastic phase IV, at 130 K; (b) in the close vicinity of the III ← II phase transition (the phase front is visible at the edges of plate); (c) in the paraelastic phase II.

(This figure is in colour only in the electronic version)

### *3.6. NMR*

The $M_2$ second moment values are shown in figure 10. $M_2$ is decreasing over the low temperature region from 4.2 $G^2$ at 77K to about 0.8 $G^2$ at 140 K and then is constant up to 296 K. This magnitude is very close to that observed in tetramethylammonium chloride [34]. In this compound the isotropic tumbling of the $[(CH_3)_4N]^+$ cation and the combined effects of lattice expansion and increasing amplitude of vibration of the ions about their normal lattice sites are considered. The analysis of the temperature dependence of the second moment for $[(CH_3)_4N]_3[As_2Br_9]$ was made on the basis of the BPP approach:

$$M_2 = M_2^{\mathrm{II}} + \left(M_2^{\mathrm{I}} - M_2^{\mathrm{II}}\right)\frac{2}{\pi}\tan^{-1}\left(\gamma\sqrt{M_2}\tau_c\right) \tag{3}$$

where $\tau_c = \tau_0 \exp\left(\frac{E_a}{RT}\right)$, $M_2^{\mathrm{I}}$ and $M_2^{\mathrm{II}}$ are the second moment values before and after the onset of a given motion, respectively. From this fitting procedure the following parameters were obtained: activation energy 0.87 kcal $mol^{-1}$ and correlation time about $3.0 \times 10^{-8}$ s. We should notice the quite small value of the activation energy barrier and the relatively slow correlation time for some molecular motion of the cation. A significant reduction in the $M_2$ value indicates the onset of the overall motion of the cations. It may justify the long correlation time estimated in this experiment.

The experimental values of $T_1$ plotted against temperature are shown in figure 11. The spin–lattice relaxation time passes through the two minima at 125 K and 185 K with $T_{1\,\mathrm{min}} = 75$ ms and $T_{1\,\mathrm{min}} = 58.2$ ms, respectively. Although the phase transitions at 165 and 171 K are hardly visible in the temperature dependence of the relaxation time as well as in the second moment, a small anomaly is visible in the dependence of $T_1$ at $1000/T$ amounting to 2.89 $K^{-1}$, i.e. $T = 346$ K, II → I phase transition. The two minima in the $T_1$ temperature dependence

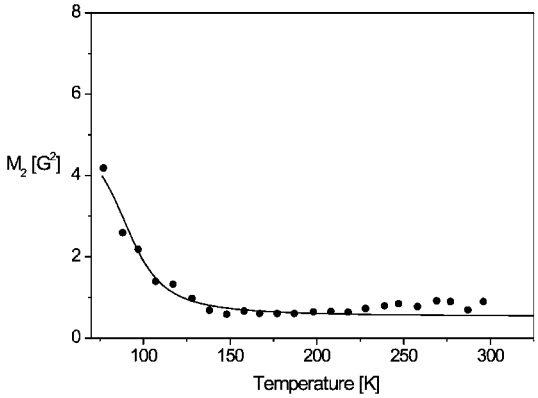


**Figure 10.** The $M_2$ second moment versus temperature.

indicate two types of motion as explained by Albert *et al* [35]. The low temperature minimum was attributed to the $C_3$ methyl group reorientations whereas the high temperature minimum was attributed to reorientational motion of the $[(CH_3)_4N]^+$ cation. The calculated spin–lattice relaxation rate including the proton–proton dipolar interactions in the methyl groups and the intra-methyl-group dipolar interactions within the same molecule is given as

$$\frac{1}{T_1} = Ag\,(\omega_0, \tau_{c2}) + Bg\,(\omega_0, \tau_{c1}) \tag{4}$$

where $g\,(\omega_0, \tau_{ci})$ are the spectral density functions and

$$A = \frac{9}{20}\frac{\gamma^4\hbar^4}{r^6}, \qquad B = \frac{3}{20}\frac{\gamma^4\hbar^4}{r^6} + \frac{27}{10}\frac{\gamma^4\hbar^4}{r_{\mathrm{TEMA}}^6}, \qquad \frac{1}{\tau_{c2}} = \frac{1}{\tau_c} + \frac{1}{\tau_{c1}}. \tag{5}$$

In these equations $\tau_c$ is the correlation time assigned to the methyl group reorientations, $\tau_{c1}$ is the correlation time of the reorientations of the whole cation, $\omega_0$ is the Larmor frequency, $r$ is the proton–proton distance within the methyl group and $r_{\mathrm{TEMA}}$ is the distance between the centres of the methyl groups within the same molecule of the cation. When $\tau_c \ll T_{1\,\mathrm{min}}$, the minimum value of $T_1$ can be written as

$$\frac{1}{T_{1,\mathrm{min}}} = \frac{9}{20}\frac{\gamma^4\hbar^4}{r^6}\frac{1.4252}{\omega_0}. \tag{6}$$

$T_{1\,\mathrm{min}}$ (equation (3)) was estimated to be 34 ms, assuming $r = 1.79$ Å. The low temperature experimental $T_1$ minimum is somewhat longer than the calculated value, which may be explained in terms of the presence of nonequivalent $[(CH_3)_4N]^+$. Taking into account their dynamic properties we can assume that the possible ratio of the cations is 2:1. Therefore the low temperature minimum may be attributed to two-thirds of all methyl groups. Below the liquid nitrogen temperature another minimum, attributed to the remaining one-third of the methyl groups, is expected. The high temperature minimum results from the isotropic tumbling of the $[(CH_3)_4N]^+$ cation. According to the above assumptions the following relation may be used [35–37]:

$$\frac{1}{T_1} = \frac{2}{3}Ag\,(\omega_0, \tau_{c2}) + Bg\,(\omega_0, \tau_{c1})\,. \tag{7}$$

The obtained values of the fitting procedure are listed in table 3.

At the phase transition at 346 K the spin–lattice relaxation time does not experience any important changes, except for a quite small jump at this temperature. Such a temperature

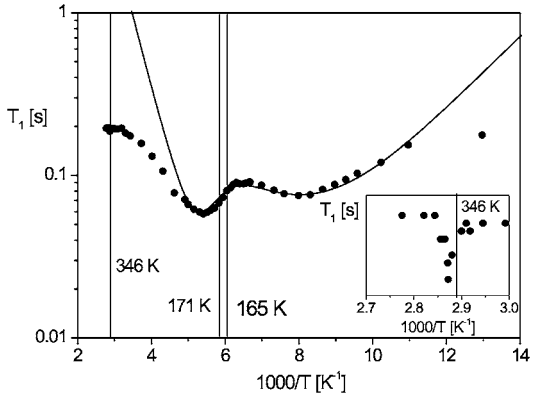


**Figure 11.** The spin–lattice, $T_1$, relaxation time versus $1000/T$. The inset is the magnification of the vicinity of the II $\leftrightarrow$ I phase transition.

**Table 3.** Motional parameters of fitting procedure.

| Motion | $\tau_0$ (s) | $E_a$ (kcal mol$^{-1}$) |
|---|---|---|
| Isotropic tumbling of cation | $1.05 \times 10^{-14}$ | 4.4 |
| $C_3$ reorientation of methyl group | $1.73 \times 10^{-11}$ | 1.02 |

characteristic of $T_1$ proves that the dynamics of the tetramethylammonium moieties play a minor role in the phase transition mechanism at 346 K.

## 4. Discussion

$[(CH_3)_4N]_3[As_2Br_9]$ appears to crystallize at room temperature in the trigonal, polar space group: $P31c$. The crystal structure is characterized by the presence of discrete bioctahedral $[As_2Br_9]^{3-}$ units and weakly distorted tetramethylammonium cations. The cationic moieties placed in the special positions on a triad axis were found to be highly disordered. A significant dynamical disorder of the cations forces a high symmetry of the crystal. The freezing of the orientational cation motion with decreasing temperature should lead to lowering of the local symmetry of the cation, and consequently to a change in the symmetry of the crystal. In the case of $[(CH_3)_4N]_3[As_2Br_9]$, such a situation takes place at low temperatures. It is interesting that the bromine analogue appears to be isomorphous to the chlorine one [17]. The isomorphism of both crystals is well reflected in their dielectric properties; however, the phase situation is a bit different. The sequence of the phase transitions in two tetramethylammonium arsenate(III) analogues is compared below:

$$\underset{ferroelastic\ II}{\overset{146\ \mathrm{K}}{|}} \xrightarrow[\text{paraelastic } I]{P31c} [(CH_3)_4N]_3[As_2Cl_9]$$

$$\underset{ferroelastic\ IV}{\overset{158\ \mathrm{K}}{|}} \underset{ferroelastic\ III}{\overset{163\ \mathrm{K}}{|}} \xrightarrow[\text{paraelastic } II]{P31c} \overset{346\ \mathrm{K}}{|} \xrightarrow[\text{symmetry } I]{hexagonal} [(CH_3)_4N]_3[As_2Br_9]$$

Despite structural similarities of both compounds (identical disorder of the organic cations at room temperature) the phase situation in the bromine analogue is more complicated. To discuss and compare the molecular mechanism of phase transitions in two isomorphic

tetramethylammonium analogues we should consider which kind of motion contributes mainly to the phase transition mechanism at low temperatures. On the basis of single-crystal x-ray diffraction and dielectric studies we can state, without any doubts, that the tetramethylammonium cations are believed to contribute to an 'order–disorder' mechanism of phase transitions of both compounds.

The differentiation between 'displacive' and 'order–disorder' transition mechanisms is possible on the basis of both the x-ray data and the transition entropy ($\Delta S_{tr}$) magnitude accompanying the low temperature phase transitions. The sum of $\Delta S_{tr}$ of two closely lying transitions at 163 and 158 K of the bromine analogue was estimated to be about 8.3 J mol$^{-1}$ K$^{-1}$ and about 13.7 J mol$^{-1}$ K$^{-1}$ for the chlorine one. The $\Delta S_{tr}$ magnitude for both crystals is characteristic of the 'order–disorder' mechanism. Probably in the bromine compound the ceasing of the motion of cations undergoes two steps, which is understood in the presence of various kinds of tetramethylammonium cations. However, in the chlorine compound the freezing of motion of all types of cations takes place simultaneously at 146 K (two-site model for three cations). Taking into account the $\Delta S_{tr}$ for the bromine crystal we can assume the freezing of two of three nonequivalent cations close to 163 and 158 K. Significant dynamic disorder of the tetramethylammonium cations precludes proposing a clear model for the motion of cations in the trigonal room temperature phases of $[(CH_3)_4N]_3[As_2Br_9]$.

The dynamical differentiation of the cations is rather negligible in the case of the chlorine compound, whereas it is enhanced in the bromine one. This evidently leads to the two well separated phase transitions and two dielectric relaxators disclosed in the dielectric response of the $[(CH_3)_4N]_3[As_2Br_9]$ crystal. Both compounds were found to exhibit a relaxation process in the kilohertz frequency region with rather small dielectric increments ($\Delta\epsilon$) of the order of two to three units along the *c*-axis. The activation energy estimated from the dielectric dispersion studies for the tetramethylammonium cation motion ranges from 47 to 20 and 12 kJ mol$^{-1}$ for the chlorine and bromine analogues, respectively. It should be emphasized that $[(CH_3)_4N]_3[As_2Br_9]$ is characterized by a significant dielectric anisotropy. This means that the dipolar and quite symmetrical cations are not expected to perform the free isotropic rotation since a different projection of the resultant dipole moment of the unit cell on the *c* and *a*-axis was observed. This seems to be consistent with the calorimetric results. The high temperature phase transition in $[(CH_3)_4N]_3[As_2Br_9]$ at 346 K is, most likely, a 'displacive' type because the motional state of the organic cations persists unchanged through the II $\rightarrow$ I phase transition. This suggestion is in agreement with a negligible thermal effect which is recorded in the DSC experiment.

It is interesting that from a structural point of view tetramethylammonium arsenates(III) are closer to the tetramethylphosphonium halogenoantimonates(III) and halogenobismuthates(III) crystallizing with the same space group $P31c$, whereas all the halogenoantimonates(III) and halogenobismuthates(III) containing the tetramethylammonium cations were found to appear in the hexagonal symmetry: $P6_3/mmc$. The latter subgroup of compounds crystallizes in the room temperature phase in the nonpolar space group, which is the basic feature which distinguishes these two subgroups of salts.

The most specific and common feature characterizing all tetramethylammonium and tetramethylphosphonium analogues is the presence of the ferroelastic properties in their low temperature ordered phases. The quaternary cations are characterized by a tendency to exhibit a high dynamic disorder at room temperature. The change in the dynamical state of the cations situated on the special positions breaks the symmetry of crystals, which takes place at the low temperature phase transitions. As a result, a disappearance of the triad or sixfold axes, understood as a lowering of the crystallographic symmetry, has to lead to the appearance of the ferroelastic structure. In all cases the x-ray diffraction pattern usually reveals a lowering of the

symmetry. This is due to a clear twinning upon cooling and therefore it was rather impossible to determine the symmetry of the ferroelastic phases.

It was shown that in all tetramethylphosphonium and tetramethylammonium arsenate(III) analogues the low temperature phase transitions ($P31c \rightarrow$ monoclinic(?)) are usually accompanied by significant changes in the spontaneous polarization magnitude of the order of $1 \times 10^{-4}$, which is characteristic of weak ferroelectrics. Unfortunately, the spontaneous polarization does not appear to be reversible, because of either the high coercive field or breaking of the single crystals undergoing the phase transition.

In general, the reorientational disorder of the organic moieties is well reflected in the proton magnetic resonance measurements, but observed effects are quite subtle. Two types of motion were detected: the $C_3$ type reorientations of the $CH_3$ group at low temperatures and the tumbling of the cations (isotropic rotation) at high temperatures. The former motion is not visible both in the x-ray and the dielectric experiments, whereas the tumbling of the cations seems to be confirmed by the presence of the dielectric relaxation process. The correlation time obtained from the second moment analysis ($3 \times 10^{-8}$ s) is comparable with that estimated from the dielectric function (macroscopic relaxation time—$10^{-8}$–$10^{-7}$ s).

The $^1$H NMR studies on $[(CH_3)_4N]_3[As_2Br_9]$ show that the low temperature phase transitions are hardly visible, which suggests rather subtle changes in the motional state of the $[(CH_3)_4N]^+$ cations through the transition ($\Delta S \approx 8.3$ J mol$^{-1}$ K$^{-1}$). On the other hand, the higher temperature transition at 346 K is better visible in $T_1$ versus $T$ measurements, which indicates the cations' contribution to the mechanism of this transition.

## Acknowledgment

This work was supported by the Polish State Committee for Scientific Research (project register 3 T09A 023 26).

## References

[1] Sobczyk L, Jakubas R and Zaleski J 1997 *Polish J. Chem.* **71** 265
[2] Jakubas R, Bator G and Ciunik Z 2003 *Phys. Rev.* B **64** 024103
[3] Kulicka B, Kinzhybalo V, Jakubas R, Ciunik Z, Baran J and Medycki W 2006 *J. Phys.: Condens. Matter* **18** 5087
[4] Jakubas R, Piecha A, Pietraszko A and Bator G 2005 *Phys. Rev.* B **72** 104107
[5] Bujak M and Zaleski J 2004 *J. Solid State Chem.* **177** 3202
[6] Bujak M and Angel R J 2005 *J. Solid State Chem.* **178** 2237
[7] Jakubas R and Sobczyk L 1990 *Phase Transit.* **20** 163
[8] Jóźków J, Jakubas R, Bator G and Pietraszko A 2001 *J. Chem. Phys.* **114** 7239
[9] Carpentier P, Lefebvre J and Jakubas R 1995 *Acta Crystallogr.* B **51** 167
[10] Jakubas R, Czapla Z, Galewski Z, Sobczyk L, Zogał O J and Lis T 1986 *Phys. Status Solidi* a **93** 449
[11] Zaleski J and Pietraszko A 1996 *Acta Crystallogr.* B **52** 287
[12] Wojtaś M, Jakubas R, Ciunik Z and Medycki W 2004 *J. Solid State Chem.* **177** 1575
[13] Aureivilius A and Stalhandse C 1978 *Acta Chem. Scand.* A **32** 715
[14] Jakubas R and Sobczyk L 1988 *Ferroelectrics* **78** 69
[15] Medycki W, Jakubas R, Piślewski N and Lefebvre J 1993 *Z. Naturf.* a **48** 748
[16] Wojtaś M, Ciunik Z, Bator G and Jakubas R 2002 *Z. Anorg. Allg. Chem.* **628** 516
[17] Wojtaś M, Bator G and Ciunik Z 2004 *Z. Anorg. Allg. Chem.* **630** 407
[18] Chen Z Y and Walker M B 1990 *Phys. Rev. Lett.* **65** 1223
[19] Cummins H Z 1990 *Phys. Rep.* **185** 211
[20] Perrez-Mato J M, Etxebarria I and Madariaga G 1991 *Phys. Scr.* T **39** 81
[21] Madariaga G, Zuniga F, Perez-Mato J M and Tello M 1987 *Acta Crystallogr.* B **43** 356
[22] Jakubas R, Bator G and Mróz J 1995 *Acta Phys. Polon.* A **87** 663
[23] Oxford Diffraction 2004 CrysAlis CCD, data collection GUI for CCD and CrysAlis RED, CCD data reduction GUI, versions 1.171.24

[24] Sheldrick G M 1997 *SHELXS–97, Program for the Solution of Crystal Structure* University of Göttingen, Germany
[25] Sheldrick G M 1997 *SHELXL–97, Program for the Refinement of Crystal Structure* University of Göttingen, Germany
[26] Sheldrick G M 1990 *SHELXTL, Siemens Analytical X-ray Instrument Inc.* Madison, WI, USA
[27] Wojtaś M 2004 *PhD Thesis* Faculty of Chemistry UWr, Wrocław
[28] McCullough J D 1964 *Acta Crystallogr.* **17** 1067
[29] Morosin B and Graeber E J 1967 *Acta Crystallogr.* **23** 766
[30] Capasso S, Giordano F and Zagari A 1983 *Acta Crystallogr.* C **39** 216
[31] Darriet J, Xu Q and Tressaud A 1987 *Acta Crystallogr.* C **43** 224
[32] Cole K S and Cole R H 1941 *J. Chem. Phys.* **9** 341
[33] Wadhavan V K 1991 *Phase Transit.* **34** 3
[34] Andrew E R and Canepa P C 1972 *J. Magn. Reson.* **7** 429
[35] Albert S, Gutowsky H S and Ripmeester J A 1972 *J. Chem. Phys.* **56** 3672
[36] Jagadeesh B, Rajan P K, Venu K and Sastry S S 1992 *Chem. Phys.* **163** 351
[37] Jagadeesh B, Rajan P K, Venu K and Sastry S S 1993 *J. Phys. Chem. Solids* **5** 527